Development and Experimental Validation of an Unglazed Photovoltaic-Thermal Collector Modelica Model that only needs Datasheet Parameters

Lone Meertens^{1*} Jelger Jansen¹ Lieve Helsen^{1,2}

¹Faculty of Engineering Science, Department of Mechanical Engineering, KU Leuven, Belgium. *Corresponding author: lone.meertens@kuleuven.be

²EnergyVille, Thor Park 8310, 3600 Genk, Belgium.

Abstract

This work introduces the first validated, user-friendly, and accurate open-source photovoltaic-thermal (PVT) collector model in Modelica, tailored for system-level simulation and optimization. Current state-of-the-art PVT collector Modelica models are largely limited to oversimplified, steady-state representations that fail to capture the dynamic thermal behavior inherent to real PVT systems. A comprehensive Modelica model is developed based on the ISO 9806 standard (test method for the quasi-dynamic thermal performance of solar thermal collectors), coupled with an electrical system model through an internal heat transfer coefficient. The model calibration relies exclusively on manufacturer datasheet parameters, thereby eliminating the need for parameter estimation from measurement data. The model is validated using experimental results from an unglazed PVT collector, demonstrating strong agreement for various (weather) conditions. The findings highlight that, while steady-state models may suffice for conventional solar thermal collectors (STCs), accurate PVT modeling necessitates a dynamic approach. particularly for the thermal aspects. The electrical output of the PVT collector is less sensitive to transient effects. In addition to the model formulation and validation, this work presents a user-friendly automated calibration method based on manufacturer data, and critically addresses the limitations and potential trade-offs of using exclusively datasheet-derived parameters, thereby providing a transparent tool for PVT system simulation, design, and optimization within the open-source IDEAS library.

Keywords: Photovoltaic-thermal (PVT) solar collector, Modelica, PVT model validation, PVT model calibration, manufacturer datasheets

1 Introduction

Physics-based system models are key for addressing the challenges of climate change and the transition towards decarbonized energy systems. These models play a key role in the effective deployment of renewable energy sources (RES) such as photovoltaic (PV), solar thermal collectors (STC), and photovoltaic-thermal (PVT) sys-

tems, enabling optimal system design and control. PVT collectors, also known as hybrid solar collectors, simultaneously convert solar radiation into electricity and heat. A key distinction exists between glazed and unglazed PVT collectors: glazed collectors often prioritize thermal efficiency, while unglazed collectors, due to their lower operating temperatures, can enhance electrical efficiency. This paper focuses on unglazed (so-called WISC¹) PVT collectors, which consist of a PV module coupled with a heat exchanger and may include rear insulation to reduce heat loss. Variants without insulation perform particularly well under sub-ambient conditions, making them suitable as heat sources for heat pump systems. The unglazed collectors are typically classified according to their rear insulation and heat transfer characteristics (Lämmle et al. 2020). The favorable market conditions for unglazed PVT designs further demonstrate their relevance in various urban and industrial energy contexts (Kramer, Amrizal, et al. 2020). Modeling approaches in the PVT field range from highly accurate, detailed, component-level models to simplified methods designed for integrated system performance assessment within a broader energy context. Although Modelica is a powerful modeling language for developing interdisciplinary simulation models, no validated open-source Modelica PVT model currently exists that captures the full dynamic thermal behavior while accounting for the thermal-electrical coupling. This paper addresses this gap by presenting a novel Modelica PVT collector model, validated using experimental data from unglazed PVT collector. Moreover, the PVT model relies solely on publicly available manufacturer data, avoiding complex calibration procedures for which measurement data are needed.

2 Background

The IEA SHC Task 60 "Application of PVT Systems" (2018–2020) has played a central role in evaluating PVT technologies by focusing on system operation, collector testing, system-level simulation, and global performance assessment (IEA SHC 2018). One of its key objectives

¹Wind and/or infrared sensitive collectors

was to identify scenarios in which PVT systems provide added value compared to separate PV and solar thermal installations. To facilitate the integration of PVT systems into simulation environments and ensure broader adoption, Task 60 stresses the need for standardized input parameters that guarantee the "processability" of technical data for tools like TRNSYS, Polysun, Modelica, and SCenoCalc (Kramer, Amrizal, et al. 2020). This standardization is crucial due to potential variations in testing procedures among manufacturers (market fragmentation), making consistent component-level characterization essential. Therefore, Task 60 recommended the application of international standards, specifically ISO 9806 (ISO 9806 2013) for the thermal aspect and IEC 60904 for the PV component. To incentivize the use of these standards, established certification frameworks such as the Solar Keymark (ESTIF/SKN n.d.) utilize and promote them, with targeted extensions to address the hybrid interactions between electrical and thermal components. This includes specifying the operational mode of electricity generation, such as maximum power point (MPP) tracking or opencircuit (OC), as required by ISO 9806 (2013) which has been identified by Hofmann et al. (2010) as highly influential on the thermal output.

Existing PVT collector models can generally be categorized into (1) those requiring detailed design data and parameter estimation, and/or (2) simplified models based on datasheet parameters. Stegmann et al. (2011) developed a datasheet-based simulation model for unglazed, liquid-cooled PVT collectors, relying solely on standard test procedures and OC-tested datasheet parameters within the TRNSYS environment. In contrast, Lämmle (2018) proposed both a collector-level model in Modelica capable of capturing the detailed optical, electrical, and thermal energy flows using detailed manufacturer data, and a system-level model in TRNSYS that assesses overall performance based on empirical efficiency curves. Other approaches focus on parameter identification of ISO 9806 parameters using measurement data: Jonas et al. (2019) presented a detailed implementation and validation procedure within TRNSYS, while Veynandt, Klanatsky, et al. (2023) extended this work using data-driven grey-box models in MATLAB. Additionally, Kang (2021) developed a Modelica-based PVT model for district heating applications, but they didn't provide any implementation details. These existing models present several limitations: some are not implemented in Modelica, others lack sufficient implementation details, and many rely on parameter estimation of ISO 9806 parameters, requiring extensive measurement data. The work presented here offers an alternative by providing a Modelica-based PVT collector model that combines a high-fidelity physical representation with the simplicity of datasheet-only inputs.

The electrical operation of a PVT collector differs from standard PV IEEE rating schemes due to the influence of heat transfer fluid (HTF) flow and the resulting temperature distribution across the PV cells (Herrando, Markides,

and Hellgardt 2014; Lämmle 2018; Brottier 2019; Jonas et al. 2019). Similarly, the electricity generation mode (MP-P/OC) impacts the thermal behavior of the PVT collector (Hofmann et al. 2010). The existing equations describing the thermal and electrical performance, used as the starting point in this paper, are presented in Section 2.1 and 2.2, respectively.

2.1 Thermal modeling

The thermal part of a PVT collector is similar to a STC. Similarly, a good efficiency requires both effective solar absorption and efficient heat transfer to the HTF (Zondag 2008). Different mathematical models are used to describe the thermal performance of liquid heating collectors, depending on the collector type (glazed or unglazed) and the test method (steady-state or quasi-dynamic). ISO 9806 defines a steady-state model for glazed liquid-heating solar collectors, widely adopted in both testing and simulation. Its useful thermal power output is calculated by Equation 1

$$\frac{\dot{Q}_{\text{th}}}{A_G} = \eta_{0,\text{hem}} G - a_1 \left(\theta_m - \theta_a\right) - a_2 \left(\theta_m - \theta_a\right)^2, \quad (1)$$

where \dot{Q}_{th} is the useful thermal power output (W), A_G is the collector area (m²), $\eta_{0,hem}$ is the zero-loss (optical) efficiency for hemispherical irradiance (–), G is the global irradiance on the collector plane (W m⁻²), θ_m and θ_a are the mean HTF and ambient air temperatures (K or °C). a_1 and a_2 are the linear and quadratic heat-loss coefficients (W m⁻² K⁻¹ and W m⁻² K⁻², respectively).

For unglazed collectors under steady-state conditions, wind-speed and long-wave effects must be included. One convenient formulation replaces G by a net solar irradiance G'', which integrates the long-wave irradiance:

$$\frac{\dot{Q}_{\text{th}}}{A_G} = G'' \Big[\eta_{0,\text{hem}} (1 - b_u) - (b_1 + b_2 u) \frac{\theta_m - \theta_a}{G''} \Big], \quad (2)$$

with
$$G'' = G + \frac{\varepsilon}{\alpha} (E_L - \sigma \theta_a^4)$$
 (3)

Here, b_u is the collector efficiency coefficient (wind dependence) (s m⁻¹), b_1 is the linear heat-loss coefficient (W m⁻² K⁻¹), b_2 is the wind-speed dependence of the heat-loss coefficient (W s m⁻³ K⁻¹), u is the wind speed, E_L is the long-wave irradiance (W m⁻²), and σ is the Stefan–Boltzmann constant.

To capture both unglazed/glazed types and transient effects, the quasi-dynamic model adds a thermal capacitance, dependence of direct (G_b) and diffuse (G_d) radiation via incidence-angle modifiers (K_b, K_d) , and explicit wind/infrared terms:

$$\frac{\dot{Q}_{th}}{A_G} = \eta_{0,b} K_b(\theta_L, \theta_T) G_b + \eta_{0,b} K_d G_d - c_1 (\theta_m - \theta_a)
- c_2 (\theta_m - \theta_a)^2 - c_3 u (\theta_m - \theta_a)
+ c_4 (E_L - \sigma \theta_a^4) - c_5 \frac{d\theta_m}{dt} - c_6 u G.$$
(4)

The quasi-dynamic model extends the steady-state form by including coefficients c_1 and c_2 , linear and quadratic

heat-loss terms analogous to a_1 , a_2 in Equation 1, with units W m⁻² K⁻¹ and W m⁻² K⁻²; c_3 and c_6 , representing wind-speed dependence of heat losses and zero-loss efficiency, with units J m⁻³ K⁻¹ and s m⁻¹; c_4 , the sky temperature dependence of the heat-loss coefficient (-); and c_5 , the effective thermal capacitance, with unit J m⁻² K⁻¹.

Equations 1–4 were originally developed for STCs, but are commonly applied to describe the thermal behavior of PVT systems, as no dedicated PVT testing standard currently exists. Depending on the test method (unglazed) steady-state or quasi-dynamic, manufacturer datasheets list all coefficients needed to solve the corresponding equation that gives the collector's thermal output under specific operational and ambient conditions. Due to the strong coupling between thermal and electrical performance in PVT systems, the thermal coefficients should ideally be determined under MPP conditions. If testing is performed under OC conditions, the solar irradiance must be corrected to account for the electrical power that would be extracted under MPP operation, as outlined by Lämmle (2018).

2.2 Electrical modeling

In PVT collectors, the electrical performance is highly sensitive to the temperature of the PV cells, which is influenced by the thermal coupling between the PV layer and the HTF in the STC. A low thermal resistance between the PV cells and the HTF is essential to avoid excessive PV cell temperatures, which degrade both electrical and thermal efficiency (Zondag 2008). This section focuses on two key aspects: the calculation of electrical yield using performance ratios, and the modeling of the PV(T) cell temperature, which plays a central role in determining the electrical output.

2.2.1 Electrical yield

The general form of the electrical power output from a PVT collector is given by Equation 5

$$\frac{P_{\rm el}}{A_G} = \eta_{\rm PV} \cdot PR_{\rm tot} \cdot G,\tag{5}$$

where η_{PV} is the electrical efficiency at nominal conditions (–), PR_{tot} is the overall instantaneous performance ratio (–), and G is the global solar radiation on the PVT plane (W).

The typical loss mechanisms affecting the electrical performance of PV and PVT systems are detailed and summarized in Kramer, Amrizal, et al. (2020), with their corresponding performance ratios $PR_{\rm IAM}$, PR_G , PR_T , PR_C and PR_I denoting incidence-angle modifier losses, irradiance-related losses, PV cell temperature losses, ohmic (cable) losses and inverter efficiency losses, respectively. In this work, only the temperature-related performance ratio PR_T is explicitly modeled. All other losses are grouped into a single lumped loss factor, as discussed in Section 3.1.3.

The temperature dependence of the electrical efficiency

is calculated following the approach by Skoplaki and Palyvos (2009) as formulated in Equation 6

$$PR_T = 1 - \beta \cdot (T_{\text{cell}} - T_{\text{nom}}), \tag{6}$$

where β is the temperature coefficient of power for the PV cells (% K⁻¹), T_{cell} is the PV cell temperature, and T_{nom} is the nominal cell temperature under standard test conditions.

2.2.2 PV cell temperature

An essential step in assessing PV efficiency and electrical yield is determining the PV cell temperature, since higher temperatures reduce performance (see Equation 6). In PV modules, cell temperature follows the module's steady-state temperature (Lämmle 2018), whereas in PVT collectors it is governed by the HTF temperature.

Solar radiation absorbed by a PV cell is partly converted to electricity; the remainder is dissipated to the ambient, influenced by wind speed, ambient temperature, and irradiance. Mounting-type-dependent cell-temperature models are reviewed in Maier et al. (2023).

A simple PVT estimate equates $T_{\rm PV}$ to the fluid outlet temperature $T_{\rm fluid,out}$ (Brottier 2019), as implemented in tools such as Polysun. A more accurate method extends the Hottel–Whillier–Bliss equation with a PV–fluid heat-transfer coefficient $U_{\rm AbsFluid}$ (Florschuetz 1976; Zondag 2008; Jonas et al. 2019).

Based on Lämmle (2018) and Jonas et al. (2019), the model couples the ISO 9806 quasi-dynamic thermal collector (Equation 4) with a two-node PV performance formulation (see Section 3.1.1), linking the PV cell and the HTF via $U_{\rm AbsFluid}$ (W m⁻² K⁻¹) to yield the cell-temperature relation in Equation 7

$$T_{\text{cell}} = T_m + \frac{\dot{q}_{\text{th}}}{U_{\text{AbsFluid}}},$$
 (7)

where $\dot{q}_{\rm th}$ is the specific thermal power output of the collector (W m⁻²), and T_m is the mean HTF temperature (K), calculated as the average of the HTF inlet and outlet temperatures, T_{in} and T_{out} respectively.

In principle, $U_{AbsFluid}$ can be calculated from the series combination of the absorber-to-pipe conductive resistance, characterized by the conductive heat transfer coefficient U_{AbsPipe} , and the pipe-to-fluid convective resistance, characterized by the convective heat transfer coefficient $U_{\text{PipeFluid}}$, based on the collector geometry, material properties, and operational conditions (e.g., fluid flow rate) using analytical models or finite-element (FEM) simulations (Kramer, Amrizal, et al. 2020). However, for most commercial PVT collectors, the absorber-specific parameters required for such detailed modeling are not readily available, as only standardized test reports or manufacturer data are typically accessible. In such cases, an approximate approach needs to be applied. Stegmann et al. (2011) developed an approach for unglazed PVT collectors, using thermal parameters extracted from OC tests. Lämmle (2018) similarly proposed a procedure for glazed PVT collectors that derives U_{AbsFluid} from standard MPP test data using a makeshift procedure. In this work, the glazed and unglazed parameter estimation methods are integrated in the Modelica model, such that $U_{\rm AbsFluid}$ can be derived solely from manufacturer datasheet parameters for MPP tested collectors, including wind-speed dependence. Details of this method are given in Section 3.1.2.

2.3 Novelty of the work

Existing PVT modeling approaches (Lämmle 2018; Jonas et al. 2019) provide robust frameworks for simulating PVT systems. However, these models typically rely on detailed parameter identification procedures or proprietary datasets, often requiring experimental calibration, finite element modeling, or surface temperature measurements. While such methods can yield high accuracy, they limit accessibility and replicability for broader research and system simulations, hinder transparent product comparisons, and ultimately restrict the market uptake of PVT technology. Furthermore, existing simplified (non-validated) Modelica models often fail to capture the full dynamic thermal behavior of PVT systems and do not adequately integrate the coupling between thermal and electrical components. For instance, Stegmann et al. (2011) proposed a simplified model based on datasheet parameters, but this model is not implemented in Modelica and is strictly limited to unglazed PVT collectors, as it relies on the steadystate ISO 9806 formulation for unglazed collectors (see Equation 2) rather than the more general quasi-dynamic approach.

In summary, the current literature regarding PVT modeling has two main research gaps: (1) the absence of a PVT model that leverages only publicly available datasheet parameters thereby eliminating the need for unavailable or proprietary measurement data, and (2) the absence of a comprehensive Modelica model that accurately represents the full dynamic thermal behavior of PVT systems while incorporating thermal-electrical coupling.

In this work, a novel Modelica-based PVT collector model is introduced and validated with experimental data from unglazed PVT collectors. Unlike previous approaches, the proposed model relies solely on datasheet parameters, thereby eliminating the need for complex calibration procedures. Moreover, the model's performance is critically assessed, highlighting its limitations and comparing its accuracy against methods based on detailed parameter estimation.

3 Model development

In this section, the methodology used to develop, implement, and validate the novel PVT collector model is presented. In Section 3.1, the underlying modeling framework is detailed while in Section 3.2, the metrics employed to assess model accuracy are discussed.

3.1 PVT collector model

The PVT collector model consists of two coupled submodels—thermal and electrical—which are detailed in Sections 3.1.1–3.1.3. To account for the changing HTF temperature along the length of the collector, the model is discretized into n_{Seg} segments along the flow path. Each segment is solved in a coupled thermal–electrical loop. For clarity, the core segment index is omitted in the equations presented in the following subsections.

3.1.1 Thermal performance

To model the thermal behavior of PVT collectors, a two-node, one-capacitance network is adopted (schematically presented in Figure 1), extending the ISO 9806 solar-thermal formulation. An internal heat transfer coefficient $U_{\rm AbsFluid}$ couples the mean HTF temperature node T_m and the absorber (PV cell) temperature $T_{\rm cell}$. All physical heat capacities (fluid, absorber, frame, insulation) are lumped into an effective thermal capacity $c_{\rm eff}$, which is assigned to the mean HTF temperature T_m (Fischer and Müller-Steinhagen 2009). Physically, this means that the thermal inertia of the entire collector system is at one uniform temperature T_m .

The T_m -node energy balance is formulated by Equation 8

$$c_{\text{eff}} \frac{dT_m}{dt} = \dot{q}_{\text{rad}} - \dot{q}_{\text{loss}} - \dot{q}_{\text{th}}, \tag{8}$$

where $\dot{q}_{\rm rad}$ are radiative gains (W m⁻²), $\dot{q}_{\rm loss}$ conduction/convection losses (W m⁻²), and $\dot{q}_{\rm th}$ the useful thermal output per area (W m⁻²). Rearranging Equation 8 and substituting the radiative gain and loss terms from Figure 1 yields: (1) the steady-state ISO 9806 model (Equation 1), by setting $c_{\rm eff}=0$ and including only the blue terms. (2) the quasi-dynamic ISO 9806 model (Equation 4), by retaining $c_{\rm eff}$ and adding the red wind-speed and sky-temperature terms.

The ISO 9806 thermal network model (dashed lines in Figure 1) is available in the open-source IBPSA Modelica library for simulating STC behavior (Wetter et al. 2019), where it is based on a simplified version of the quasi-dynamic ISO 9806 model (Equation 4) with $c_3 = c_4 = c_6 = 0$, thus neglecting wind and sky-temperature dependencies. This existing implementation serves as the starting point for the PVT collector model developed in this work. To extend its validity to unglazed collectors, wind-speed and long-wave loss terms are in-

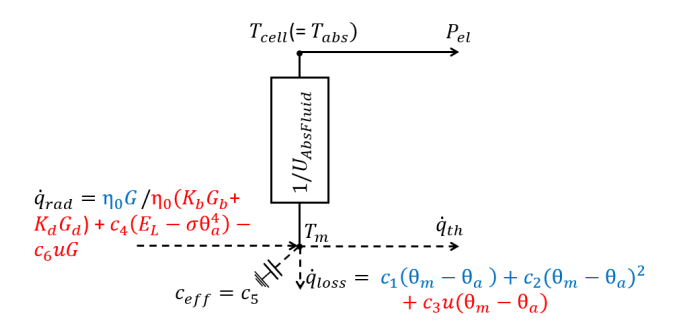


Figure 1. Two-node, one-capacitance thermal network for PVT collectors (ISO 9806: dashed lines; extension: solid lines).

corporated, resulting in the quasi-dynamic formulation (Equation 4), which captures the effects relevant for unglazed PVT thermal operation (Stegmann et al. 2011; Fischer and Müller-Steinhagen 2009). Compared to a two-node, two-capacitance network², this two-node, single-capacitance approach is ISO-compliant, simpler, and directly uses standardized parameters—and has been demonstrated as the preferred method for the PVT collectors investigated by Jonas et al. (2019).

The specific thermal output is calculated as:

$$\dot{q}_{\rm th} = \frac{\dot{m}c_p \left(T_{\rm out} - T_{\rm in}\right)}{A_G},\tag{9}$$

where \dot{m} is the mass flow rate (kg s⁻¹) and c_p the HTF specific heat capacity (kJ kg⁻¹ K⁻¹).

3.1.2 Thermal-electrical coupling

Both numerical and experimental approaches can be used to determine U_{AbsFluid} for a specific absorber design. However, the absorber-specific parameters required by these methods are rarely available for commercial PVT collectors, where test reports and datasheets are usually the only information source. PVT models that rely on parameter estimation typically fit U_{AbsFluid} alongside other thermal and electrical parameters. Since this work aims to develop an accurate PVT model based solely on datasheet inputs, a datasheet-based derivation of $U_{AbsFluid}$ is proposed by merging two established approaches. Stegmann et al. (2011) derived U_{AbsFluid} from OC-mode thermal tests (including wind-speed dependence) making it valid for unglazed collectors. Lämmle (2018) generalized this to MPP-mode glazed collectors but they omitted wind effects. The MPP-mode approach is preferred because the electrical operating point significantly influences thermal performance; if only OC-mode parameters are available, the corresponding MPP coefficients can be obtained via the conversion procedure of Lämmle (2018), which properly accounts for the coupling between electrical and thermal losses and avoids physically incorrect simplifications (Kramer and Helmers 2013).

Combining these two methods yields a unified, wind-dependent formulation using MPP datasheet coefficients:

$$U_{\text{AbsFluid}} = \frac{\left[(\tau \alpha)_{\text{eff}} - \eta_{0,\text{el}} \right] \left(c_1 + c_3 u + b_{1,\text{el}} \right)}{\left[(\tau \alpha)_{\text{eff}} - \eta_{0,\text{el}} \right] - \left(1 - \frac{c_6}{\eta_{0,\text{th}}} u \right) \eta_{0,\text{th}}}.$$
 (10)

Here $(\tau\alpha)_{\rm eff}=0.901$ for unglazed PVT collectors as reported in Lämmle (2018), and the electrical temperature-dependence coefficient is given by $b_{1,{\rm el}}=|\beta|\,G_{\rm nom}$, where β is the temperature coefficient in % K⁻¹ and $G_{\rm nom}=1000\,{\rm W\,m^{-2}}$. When computed across varying wind speeds u, the resulting $U_{\rm AbsFluid}$ values should remain approximately constant, serving as a consistency check on the datasheet parameters (Stegmann et al. 2011).

3.1.3 Electrical performance

The electrical output power $P_{\rm el}$ is calculated using the PVWatts V5 formulation (Dobos 2014) as presented by Equation 11

$$P_{\rm el} = P_{\rm nom} \frac{G}{G_{\rm nom}} \left[1 + \gamma (T_{\rm cell} - T_{\rm nom}) \right] (1 - P_{\rm loss}), \quad (11)$$

where P_{nom} is the module's rated DC power under standard test conditions ($G_{\text{nom}} = 1000 \text{ W m}^{-2}$, $T_{\text{nom}} = 25 \,^{\circ}\text{C}$), T_{cell} is the PV cell temperature from the two-node thermal model (Equation 7), and P_{loss} is a constant system loss factor covering soiling, shading, mismatch, wiring and connection losses, inverter inefficiency, light-induced degradation (LID), and availability (Dobos 2014).

The term $[1+\gamma(T_{\text{cell}}-T_{\text{STC}})]$ in Equation 11 explicitly accounts for the temperature-dependence of the electrical efficiency, similar to the performance ratio formulation in Equation 6. All remaining losses are merged into a system loss factor (P_{loss}). In this study, panels are assumed unshaded with negligible soiling, yielding a P_{loss} of 9% per Dobos (2014). Given PVT 2's higher positive electrical output tolerance (up to +5% vs. +3% for PVT 1; see Table 1), its loss factor is reduced to 7%.

3.2 Error analysis

Model validation is performed against the measurement data (Section 4) by comparing both instantaneous power and cumulative energy for the thermal and electrical outputs. Instantaneous errors are quantified using the mean absolute error (MAE) and root mean square error (RMSE), while cumulative deviations are evaluated over the full dataset. For a scale-independent assessment, normalized MAE (nMAE) and normalized RMSE (nRMSE) are also computed.

The MAE and nMAE between simulated and measured outputs are defined by Equation 12 and Equation 13 respectively.

$$MAE_{Y} = \frac{1}{n} \sum_{i=1}^{n} |Y_{sim}(t_i) - Y_{meas}(t_i)|, \qquad (12)$$

$$nMAE_Y = \frac{MAE}{\frac{1}{n}\sum_{i=1}^{n}|Y_{\text{meas}}(t_i)|}.$$
 (13)

The RMSE and nRMSE are defined by Equation 14 and Equation 15 respectively.

$$RMSE_{Y} = \sqrt{\frac{1}{n} \sum_{i=1}^{n} (Y_{sim}(t_{i}) - Y_{meas}(t_{i}))^{2}},$$
 (14)

$$nRMSE_Y = \frac{RMSE}{\frac{1}{n}\sum_{i=1}^{n} |Y_{meas}(t_i)|}.$$
 (15)

Where, Y represents either the thermal power output $\dot{Q}_{\rm th}$ or the electrical power output $P_{\rm el}$, depending on the context.

 $^{^2}$ Some PVT models introduce a second capacitance linked to T_{cell} to represent the thermal inertia of the PV panel, but this additional capacity cannot be determined using typically available manufacturer data.

Table 1. Datasheet parameters for the two PVT collectors.

Parameters	PVT 1	PVT 2	
Electrical			
$A_{\rm gross}~({\rm m}^2)$	1.66	1.64	
$\beta(\%K^{-1})$	-0.41	-0.375	
$P_{\text{max}} (W_{\text{p}})$	280 (0/+3 %)	300 (0/+5 %)	
$\eta_{0, ext{el}}$ (%)	16.87	18.3	
Thermal			
$c_1 (\mathrm{W} \mathrm{m}^{-2} \mathrm{K}^{-1})$	7.411	10.74	
$c_2 (W m^{-2} K^{-2})$	0	0	
$c_3 (\mathrm{kJ} \mathrm{m}^{-3} \mathrm{K})$	1.7	1.1	
$c_4(-)$	0.437	0.363	
$c_5 (\mathrm{J} \mathrm{m}^{-2} \mathrm{K}^{-1})$	42200	22100	
$c_6 (\mathrm{s m^{-1}})$	0.003	0.036	
$\eta_{0, ext{th}}$ (%)	0.475	0.535	

4 Collector data and test sequences

Experimental data from two different unglazed PVT collecors, provided directly by the authors of the respective studies, are used for validation and are briefly summarized below.

The first dataset (PVT 1) was obtained from experimental measurements on an outdoor test bench at the Laboratory for Solar Energy Systems of the University of Applied Sciences (HTW Saar) in Saarbrücken, Germany. In this case, the PVT collector is an uncovered collector that features a rear cover and thermal insulation on the back of the absorber. A detailed description of this dataset and the corresponding test setup is provided in Jonas et al. (2019). The experimental measurements cover the typical days³ as defined in ISO 9806 and include both standard thermal performance measurements and continuous recordings of the relevant electrical values.

The second dataset (PVT 2) was obtained from the real operation of a flat-plate, uncovered, and uninsulated PVT collector on a test bench in Austria. This dataset spans 58 summer days (from July 11 til September 6) with a 5-second sampling interval. The data, which is publicly available, is described in detail in Veynandt, Inschlag, et al. (2023). A selection of the measured variables from this dataset has previously been used in the development of a grey-box PVT model (Veynandt, Klanatsky, et al. 2023).

Table 1 lists the datasheet parameters describing the thermal and electrical behavior of both collectors. The thermal coefficients follow the quasi-dynamic (general) test method, following Equation 4. For PVT 2, the thermal coefficients were originally obtained under the unglazed steady-state method (Equation 2) and then converted to quasi-dynamic form (Equation 4) following the approach detailed in Solar Keymark Network (2019).

As both datasets did not contain all data required to do a (one-to-one) validation of the model presented in Section 3.1, some assumptions had to be made. First, for PVT 1, the measured long-wave irradiance on the tilted plane was found to be unreliable, necessitating the estimation of long-wave radiation losses from the effective sky temperature. Only the solar irradiance components on the tilted plane were measured. Estimating cloud cover (and thus sky temperature) requires horizontal-plane irradiance data to determine the diffuse fraction. In the absence of such data, the diffuse fraction is assumed identical across all orientations. This assumption affects the sky temperature estimate and, consequently, the modeled long-wave radiation losses. Second, for PVT 2 the total irradiance on the tilted collector plane is used directly in the simulation following Equation 2; accordingly, no conversion of the datasheet value for $\eta_{0,\text{hem}}$ is necessary.

5 Results and analysis

This section is organized as follows: Section 5.1 validates the thermal and electrical performance against the measurement data introduced in Section 4, both in terms of instantaneous power and cumulative energy. Sections 5.2 and 5.3 examine how thermal and electrical parameters affect the model's accuracy.

5.1 Model validation

The accuracy of the PVT collector model is assessed against the two datasets introduced in Section 4, using only the datasheet coefficients from Table 1 to set up the PVT collector model. The evaluation of PVT 1 is based on Table 2 and Figure 3, while PVT 2 is assessed using Figure 2. The sole model parameter not directly provided in the datasheet, namely the overall absorber-fluid heat transfer coefficient $U_{AbsFluid}$, is computed for each PVT collector using Equation 10. As discussed in Section 3.1.2, Stegmann et al. (2011) argue that similar U_{AbsFluid} values across different wind speeds is indicative of robust datasheet parameters. In our case, both datasets exhibit a pronounced variation of $U_{AbsFluid}$ with wind speed, suggesting a possible inconsistency in the wind-dependent coefficients c_3 and c_6 . For the reference scenario, the wind-independent U_{AbsFluid} values for PVT 1 and PVT 2 are $32.76 \text{ W m}^{-2} \text{ K}^{-1}$ and $56.85 \text{ W m}^{-2} \text{ K}^{-1}$, respectively. Section 5.3 will further explore how the choice of $U_{\rm AbsFluid}$ affects the accuracy of the predicted electrical power out-

Table 2 reports the error metrics (introduced in Section 3.2) for PVT 1. For day types 1 to 3, thermal performance shows acceptable agreement between model and measurements, with energy deviation (ΔE) remaining below 5%. In contrast, day type 4 shows a significantly higher deviation of 36.7%, indicating model limitations under high temperature difference and low irradiance conditions (see Figure 3(d)). These discrepancies likely stem from underestimated wind-dependent losses (coefficients c_3 and c_6) and increased radiative losses due to the larger

 $^{^3}$ Day type 1: η_0 -conditions, mostly clear sky conditions.Day type 2: Elevated operating temperature or η_0 -conditions, partly cloudy conditions including broken cloud and clear sky conditions.Day type 3: Mean operating temperature conditions including clear sky conditions.Day type 4: High operating temperature conditions including clear sky conditions

HTF-to-ambient temperature difference. As the absolute thermal output is low in this case, model limitations have a stronger effect, leading to disproportionately large relative deviations. While the MAE and RMSE are lowest under clear-sky conditions, larger errors during variable-sky periods (type 2 and type 4) point to a mismatch in the dynamic response of the thermal model, involving the c_5 coefficient. Additionally, the use of a sky temperature approximation introduces uncertainty in the long-wave loss term c_4 , as noted in Section 4, and warrants closer examination. Electrical performance validation of PVT 1 yields normalized MAE and RMSE values below 3.1% (Table 2), confirming the accuracy of the electrical component of the PVT collector model.

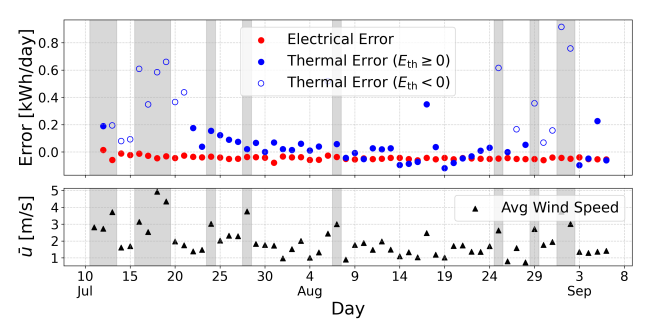


Figure 2. Top: Error between the measured and simulated daily thermal and electrical energy production of the PVT 2 collector, expressed in kWhd⁻¹, over the entire dataset. Bottom: Corresponding average wind speed during operation for each day, with high wind speed periods ($\bar{u} > 2.5 \, \text{m/s}$) indicated by the grey sections.

For PVT 2, Figure 2 compares measured and simulated daily thermal and electrical energy alongside average wind speed, and Table 2 summarizes the key error metrics. Figure 2 indicates a clear correlation between thermal energy mismatch and higher wind speeds, suggesting further investigation of the wind-dependent coefficients c_3 and c_6 . Over the full validation period at 5-s resolution the thermal model predicts 20.4 kWh vs. 13.4 kWh measured ($\Delta E = +53.1\%$), but this large error is driven by many periods of negative thermal output that would not occur in real operation. Filtering to $Q_{\text{th,sim}}(Q_{\text{th,meas}}) > 0$ yields a more realistic energy error of $\Delta E = +6.85\%$ (-4.7%). Electrical predictions remain robust (MAE: 3.2 W, ME: -1.8 W, $\Delta E = -2.9\%$, 83.8 kWh predicted vs. 86.3 kWh measured) and are essentially unaffected by wind speed.

5.2 Thermal parameters

Thermal performance is first examined for PVT 1 under controlled conditions, followed by an assessment of deviations for PVT 2 including high wind speed operation.

PVT 1: standard test conditions

Analysis is based on four representative day types (Figure 3), spanning clear to overcast skies with mean HTF-ambient temperature differences of 0 K (types 1–2), 10 K (type 3) and 20 K (type 4). An artificial blower maintained a constant wind speed of 3 m s⁻¹ to 4 m s⁻¹,

such that wind effects remain uniform across cases. The stacked loss distributions represent the individual heat loss contributions within the quasi-dynamic thermal model (Equation 4), each defined by a specific datasheet coefficient. The impact of these loss terms on thermal performance is examined in the remainder of this section. The heat-loss coefficients c_1 and c_2 are excluded from further discussion due to their negligible influence on model accuracy under the given operating conditions.

Wind-speed dependence (c_3, c_6) . In this study, wind speeds during all day type measurements (Figure 3) remained within $3 \,\mathrm{m\,s^{-1}}$ to $4 \,\mathrm{m\,s^{-1}}$, placing them at the upper edge of the ISO calibration range $(0-3.5 \,\mathrm{m/s})$ and calling the accuracy of the wind-dependent coefficients into question. The persistent steady-state error across all day types indicates an underestimation of c_6 , which is significant even for day types 1-2 where c_3 has limited impact due to small $\theta_m - \theta_a$, while c_3 becomes more influential at larger temperature differences. These findings suggest that convective losses do not scale linearly beyond the calibration range.

Sky-temperature dependence (c_4). The c_4 term accounts for radiative heat losses based on the difference between ambient air and sky temperature, expressed as $(E_L - \sigma \theta_a^4)$. This term is typically negative, with values around $-100 \, \mathrm{W \, m^{-2}}$ for clear skies, $-50 \, \mathrm{W \, m^{-2}}$ under hazy conditions, and approximately zero for overcast skies (ISO 9806 2013). In this work, the sky temperature for PVT 1 is approximated according to the assumptions in Section 4, which may introduce steady-state errors in the long-wave loss term and affect the accuracy of the thermal simulation.

Thermal capacity (c_5) . ISO 9806 limits uncertainty in HTF heat capacity to ± 10 %, yet quasi-dynamic identification often yields larger deviations (Weißmüller, Frenz, and Krämer 2012), attributable to limited variation in HTF temperature during standard tests. Calculations based on material properties and ISO weighting factors can reduce this uncertainty (Lämmle 2018). However, identified values may still fail to capture rapid irradiance transients (Stegmann et al. 2011). In this study, the datasheet c_5 is too large, slowing the model's thermal response (Figure 3) and causing notable errors during fast-changing conditions. Reducing c_5 would sharpen transients but exacerbate steady-state bias, indicating that adjustment of c_5 alone cannot resolve the dynamic mismatch.

Comparison with quasi-dynamic identification. For day types 1–2, underestimation of steady-state losses leads to overestimated thermal output, implicating the sky-temperature term c_4 and/or the wind-dependent term c_6 . A similar bias occurs in types 3–4, but larger $\theta_m - \theta_a$ elevates the influence of c_3 , while the model's slower transient response points to an overestimated thermal capacity c_5 . Compared to the parameter set identified by Jonas et al. (2019), the datasheet coefficients differ by

Table 2. Model validation results for PVT 1 and PVT 2. Computations use a 3-segment discretization, datasheet parameters, a loss factor of 9 % for PVT 1, and 7 % for PVT 2. For PVT 1, $U_{\text{AbsFluid}} = 32.76 \, \text{W} \, \text{m}^{-2} \, \text{K}^{-1}$; for PVT 2, $U_{\text{AbsFluid}} = 56.85 \, \text{W} \, \text{m}^{-2} \, \text{K}^{-1}$.

	Thermal Performance									
	MAE (W)	nMAE (%)	RMSE (W)	nRMSE (%)	ME (W)	E _{sim} (kWh)	E _{meas} (kWh)	ΔE (%)		
PVT 1 (Day type 1)	18.5	3.33	20.4	3.66	18.5	3.73	3.61	3.33		
PVT 1 (Day type 2)	91.5	18.8	132.2	27.1	10.7	3.06	2.99	2.19		
PVT 1 (Day type 3)	58.4	19.9	92.5	31.6	12.2	2.33	2.23	4.17		
PVT 1 (Day type 4)	97.4	85.7	151.2	133.0	41.7	0.78	0.57	36.7		
PVT 2	10.7	111.2	33.9	352.9	5.10	20.4	13.4	53.1		
PVT 2 ($Q_{\text{th,sim}} > 0$)	43.1	30.8	66.9	47.8	9.57	26.6	24.9	6.85		
PVT 2 ($Q_{\text{th,meas}} > 0$)	35.2	21.0	52.1	31.2	-7.86	25.5	26.8	-4.7		
	Electrical Performance									
	MAE (W)	nMAE (%)	RMSE (W)	nRMSE (%)	ME (W)	E _{sim} (kWh)	E _{meas} (kWh)	ΔE (%)		
PVT 1 (Day type 1)	1.04	0.49	1.36	0.64	0.91	1.00	1.00	0.43		
PVT 1 (Day type 2)	4.30	2.48	5.34	3.08	3.72	1.14	1.11	2.15		
PVT 1 (Day type 3)	2.80	1.61	3.43	1.97	2.35	1.29	1.27	1.35		
PVT 1 (Day type 4)	3.26	1.98	3.88	2.36	2.78	0.86	0.84	1.69		
PVT 2	3.21	5.18	6.11	9.86	-1.80	83.8	86.3	-2.91		

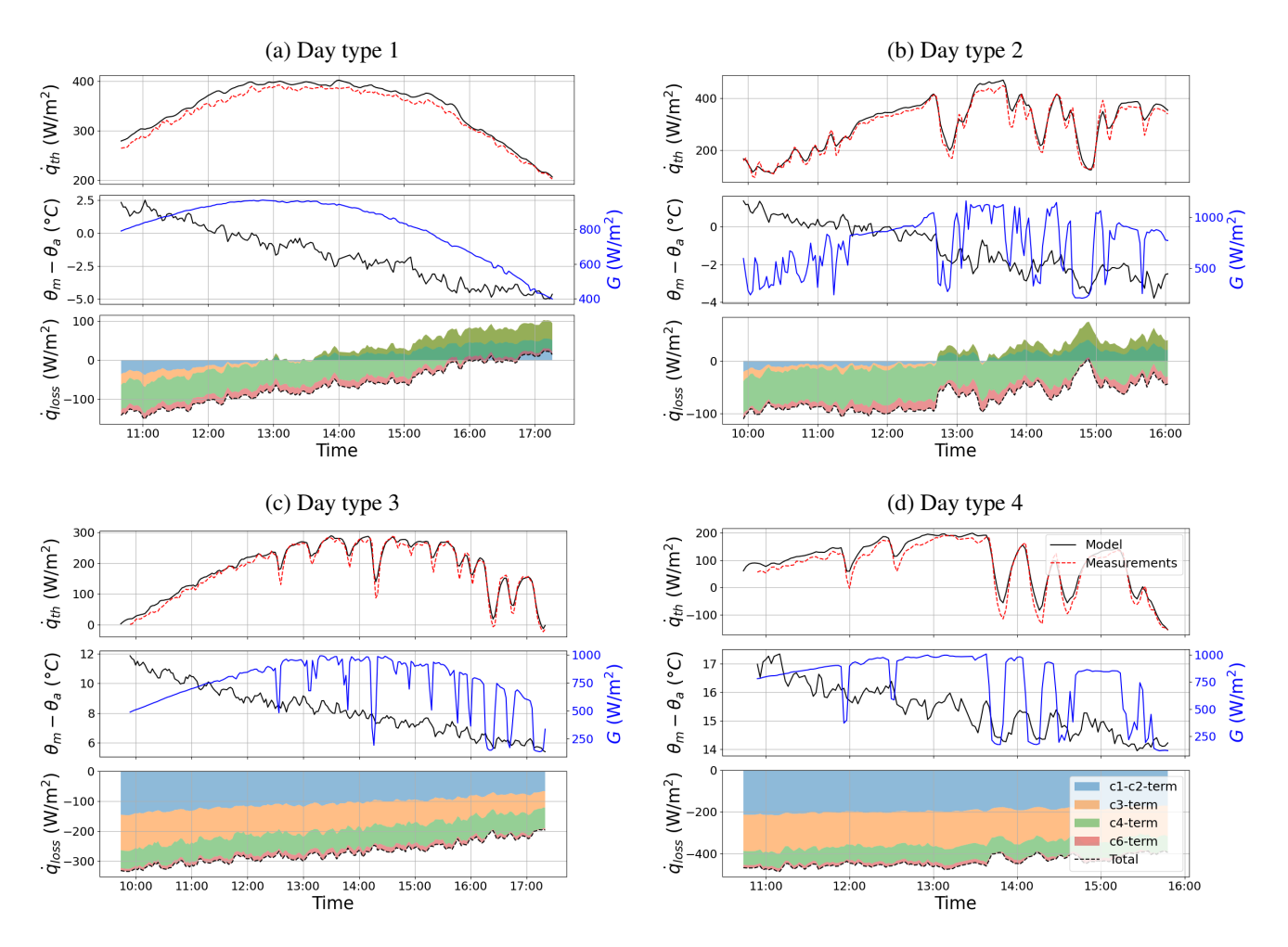


Figure 3. Comparison between simulated and measured thermal output and losses for different day types. Each subfigure shows: Top: thermal output \dot{q}_{th} (model vs. measurements); Middle: temperature difference $\theta_m - \theta_a$ and solar irradiance; Bottom: simulated thermal loss contributions and total loss. A single common legend (identical across day types) is displayed in day type 4.

 $\Delta c_3 = -1.4\%$, $\Delta c_4 = 63.1\%$, $\Delta c_5 = 11.5\%$, and $\Delta c_6 = -90.3\%$. The strong negative bias in c_6 , partly offset by a positive bias in c_4 , highlights that model limitations peak under high wind speeds, as further illustrated by the thermal behavior of PVT 2.

PVT 2: high wind conditions

As shown in Figure 2 and discussed in Section 5.1, the model systematically overestimates the thermal output of PVT 2, particularly under higher wind speeds. The collector frequently operates near its upper temperature limit, with a mean HTF-to-ambient temperature difference of 19.52 K, which is suboptimal for unglazed PVT collectors. This condition, resulting from the test setup described in Veynandt, Inschlag, et al. (2023), leads to phases of low or even negative thermal output. While not representative of typical operation, this validation is valuable for exposing model limitations.

The pronounced overestimation under high wind conditions (occasionally exceeding $10~\mathrm{m\,s^{-1}}$) suggests that the wind-dependent coefficients c_3 and c_6 do not scale linearly beyond the calibrated range. This effect is exacerbated by the uninsulated rear side of the collector, increasing its sensitivity to convective losses. Additionally, the use of a varying mass flow rate, differing from the (nominal) one used for datasheet coefficient determination, may contribute to discrepancies. Because these effects primarily affects convective heat transfer and potentially electrical performance, they will be addressed in Section 5.3.

5.3 Electrical parameters

As discussed in Section 2.2.2, the PV cell temperature strongly affects the electrical efficiency of a PVT collector (see Equation 6). To account for the influence of thermal operation on the PV cell temperature, a thermal coupling between the PV cell and the HTF is introduced via the coefficient $U_{\rm AbsFluid}$, which is formulated in Equation 7. In this work, $U_{\rm AbsFluid}$ is estimated using a simplified, datasheet-based method (Section 3.1.2). This section examines the impact of variations in the estimated $U_{\rm AbsFluid}$ on the accuracy of the modeled electrical power output.

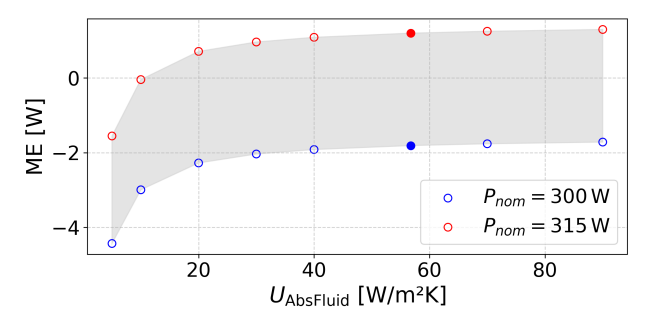


Figure 4. Mean electrical error versus $U_{\rm AbsFluid}$ for $P_{\rm nom} = 300$ W and 315 W. Filled markers denote the estimated (datasheet-based) value of $U_{\rm AbsFluid}$.

Figure 4 shows the normalized mean error in electrical output versus variations in U_{AbsFluid} for two nominal

powers: $P_{\rm nom} = 300\,\rm W$ and 315 W (reflecting a +5% tolerance; see Table 1). A constant system loss factor of 9% is applied throughout (Equation 11). As shown, a shift in $U_{\rm AbsFluid}$ has minimal effect under good thermal coupling, while the grey band, representing uncertainty from rated power tolerance and assumed $P_{\rm loss}$, causes greater deviation. The trend observed in Figure 4 aligns with Lämmle (2018), who found that values above $60\,\rm W\,m^{-2}\,K^{-1}$ indicate good coupling, with little gain beyond. Hence, a simplified datasheet-based $U_{\rm AbsFluid}$ suffices for accurate output predictions. Making it mass-flow dependent adds complexity without meaningful accuracy gains, as constant values already yield reliable results.

5.4 Model limitations

The following limitations apply primarily to unglazed PVT collectors: (1) High wind speeds: convective losses (coefficients c_3 , c_6) are increasingly underestimated above the ISO calibration range ($\approx 3.5\,\mathrm{m\,s^{-1}}$); (2) Dynamic response: thermal capacity (c_5) may be misestimated, impacting the model's transient behavior under rapidly varying irradiance. Glazed PVT collectors are not affected by (1) but remain subject to (2); this hypothesis should be investigated in future work.

6 Conclusion and future work

By offering an open-source, modular, and transparent modeling framework, this work sets a significant step toward democratizing high-fidelity PVT system simulations, thereby empowering researchers, engineers, and policymakers to optimize PVT systems without relying on proprietary tools or inaccessible data.

Validation against two experimental datasets demonstrated that the electrical sub-model achieves very good accuracy, with the nMAE and nRMSE both below 3.1% for PVT 1 (day types 1–4) and 5.2% / 9.9% for PVT 2. The thermal model reproduces daily energy within 3.3%, 2.2%, 4.2% and 36.7% for PVT 1 day types 1–4, respectively, and 6.85% for PVT 2 (excluding negative thermal output periods).

These results confirm that, except under extreme conditions, the simplified datasheet-based approach yields reliable predictions. Limitations arise primarily for unglazed collectors for high wind speeds, where convective and radiative losses are not fully captured.

Future work should validate glazed PVT collectors, whose insulation and higher operating temperatures may mitigate the limitations identified for unglazed systems. For unglazed collectors, investigations into non-linear convective formulations could better characterize the wind-dependent loss coefficients c_3 and c_6 . Refining the sky-temperature approximation is also needed to reduce steady-state radiative errors. Finally, embedding this PVT model within full energy-system simulations (e.g., district heating networks or building HVAC models) would enable end-to-end optimization of hybrid solar technologies across diverse climates and applications.

7 Data availability

The PVT model and its validation are available in the IDEAS Library: https://github.com/open-ideas/IDEAS/pull/1446. The measurement data is available in the IDEAS resources folder.

Acknowledgements

The authors acknowledge the funding by the KU Leuven C3 ASiRE² project (C3/22/029) and the European Union through the SEEDs project under the Horizon Europe Programme. Views and opinions expressed are however those of the author(s) only and do not neces- sarily reflect those of the European Union or CINEA. Neither the European Union nor the granting authority can be held responsible for them.

References

- Brottier, Laetitia (2019). "Optimisation biénergie d'un panneau solaire multifonctionnel : du capteur aux installations in situ". PhD thesis. Université Paris-Saclay (COmUE).
- Dobos, Aron P. (2014-09). *PVWatts Version 5 Manual*. Tech. rep. NREL/TP-6A20-62641, Contract No. DE-AC36-08GO28308, Prepared under Task No. SS13.5030. 15013 Denver West Parkway, Golden, CO 80401, USA: National Renewable Energy Laboratory (NREL). URL: https://www.nrel.gov/docs/fy14osti/62641.pdf.
- ESTIF/SKN (n.d.). *The Solar Keymark Scheme Rules*. http://www.estif.org/solarkeymarknew/the-solar-keymark-scheme-rules. Accessed 2024.
- Fischer, S. and H. Müller-Steinhagen (2009). "Collector efficiency testing the 2-node collector model ready for implementation in European Standard EN 12975". In: *Proceedings of the ISES Solar World Congress 2009*. International Solar Energy Society (ISES). Johannesburg, South Africa.
- Florschuetz, L. W. (1976). "Extension of the Hottel-Whillier model to the analysis of combined photovoltaic/thermal flat plate collectors". In: *Solar Energy* 22, pp. 361–366.
- Herrando, María, Christos N. Markides, and Klaus Hellgardt (2014). "A UK-based assessment of hybrid PV and solar-thermal systems for domestic heating and power: System performance". In: *Applied Energy* 122, pp. 288–309. DOI: 10. 1016/j.apenergy.2014.01.061.
- Hofmann, P. et al. (2010). "Measurements and Benchmark of PV-T Collectors According to EN 12975 and Development of a Standardized Measurement Procedure". In: *Proceedings of the EuroSun 2010 Conference*. Graz, Austria.
- IEA SHC (2018). Task 60. PVT Systems: Application of PVT Collectors and New Solutions in HVAC Systems. Official Description. https://www.iea-shc.org/task60. International Energy Agency Solar Heating and Cooling Programme.
- Jonas, Danny et al. (2019). "Performance modeling of PVT collectors: Implementation, validation and parameter identification approach using TRNSYS". In: *Solar Energy* 193, pp. 51–64. DOI: 10.1016/j.solener.2019.09.047.
- Kang, A. et al (2021). "Modeling of photovoltaic-thermal district heating with dual thermal modes". In: *Journal of Physics: Conference Series* 2042.1, p. 012090.
- Kramer, Korbinian, N. Amrizal, et al. (2020-10). *Status Quo of PVT Characterization*. Tech. rep. SHC Task 60 Report B1. Fraunhofer ISE, University of Perpignan, Dual Sun,

- University of Catania, University of Stuttgart, University of Zaragoza, Saarland University, TNO, ZAE Bayern, Czech Technical University, Dalarna University. DOI: 10.18777/ieashc-task60-2020-0004.
- Kramer, Korbinian and Henning Helmers (2013). "The interaction of standards and innovation: Hybrid photovoltaic–thermal collectors". In: *Solar Energy* 98, pp. 434–439. DOI: 10.1016/j.solener.2013.08.042.
- Lämmle, Manuel (2018-01). "Thermal management of PVT collectors: development and modelling of highly efficient glazed, flat plate PVT collectors with low emissivity coatings and overheating protection". PhD thesis. University Freiburg.
- Lämmle, Manuel et al. (2020-05). *Basic Concepts of PVT Collector Technologies, Applications and Markets*. Tech. rep. SHC Task 60/Report D5. Fraunhofer ISE, University of Zaragoza, Sunovate. DOI: 10.18777/ieashc-task60-2020-0002.
- Maier, Laura et al. (2023-10). "Comparative Study and Validation of Photovoltaic Model Formulations for the IBPSA Modelica Library based on Rooftop Measurement Data". In: *Proceedings of the Modelica Conference 2023*. Aachen, Germany. DOI: 10.3384/ecp204131.
- Skoplaki, E. and J.A. Palyvos (2009). "On the temperature dependence of photovoltaic module electrical performance: A review of efficiency/power correlations". In: *Solar Energy* 83.5, pp. 614–624. DOI: 10.1016/j.solener.2008.10.008.
- Solar Keymark Network (2019-10). *Thermal Performance Parameter Conversion to the ISO9806:2017*. URL: https://solarheateurope.eu/wp-content/uploads/2019/10/SKN-N0474R0_Thermal-performance-parameter-conversion-to-the-ISO9806-2017.pdf.
- Stegmann, M. et al. (2011). "Model of an unglazed photovoltaic thermal collector based on standard test procedures". In: *Proceedings from SWC2011: ISES Solar World Congress*. kassel (GE), 28 August 2 September 2011.
- Veynandt, François, Franz Inschlag, et al. (2023). "Measurement data from real operation of a hybrid photovoltaic-thermal solar collectors, used for the development of a data-driven model". In: *Data in Brief* 49, p. 109417. DOI: 10.1016/j.dib. 2023.109417.
- Veynandt, François, Peter Klanatsky, et al. (2023). "Hybrid photovoltaic-thermal solar collector modelling with parameter identification using operation data". In: *Energy and Buildings* 295, p. 113277. DOI: 10.1016/j.enbuild.2023.113277.
- Weißmüller, C., H. Frenz, and E. Krämer (2012-05). *Proficiency Test QAiST testing of solar collectors and solar systems 2010 2011. Final report.* Tech. rep. Final report. Daimler-straße 8, D-45770 Marl, Germany: Institut für Eignungsprüfung GmbH. URL: https://task43.iea-shc.org/data/sites/1/publications/Final%20QAiST%20Report%205-29-131.pdf.
- Wetter, M. et al. (2019-09). "IBPSA Project 1: BIM/GIS and Modelica framework for building and community energy system design and operation—ongoing developments, lessons learned and challenges". In: *IOP Conference Series: Earth and Environmental Science*. Vol. 323. Graz, Austria: IOP Publishing, p. 012114. DOI: 10.1088/1755-1315/323/1/012114.
- Zondag, H.A. (2008). "Flat-plate PV-Thermal collectors and systems: A review". In: *Renewable and Sustainable Energy Reviews* 12.4, pp. 891–959. DOI: 10.1016/j.rser.2005.12.012.